

Unsupervised Person Re-Identification with Wireless Positioning under Weak Scene Labeling

Yiheng Liu, Wengang Zhou, Qiaokang Xie, Houqiang Li, *Fellow, IEEE*

Abstract—Existing unsupervised person re-identification methods only rely on visual clues to match pedestrians under different cameras. Since visual data is essentially susceptible to occlusion, blur, clothing changes, etc., a promising solution is to introduce heterogeneous data to make up for the defect of visual data. Some works based on full-scene labeling introduce wireless positioning to assist cross-domain person re-identification, but their GPS labeling of entire monitoring scenes is laborious. To this end, we propose to explore unsupervised person re-identification with both visual data and wireless positioning trajectories under weak scene labeling, in which we only need to know the locations of the cameras. Specifically, we propose a novel unsupervised multimodal training framework (UMTF), which models the complementarity of visual data and wireless information. Our UMTF contains a multimodal data association strategy (MMDA) and a multimodal graph neural network (MMGN). MMDA explores potential data associations in unlabeled multimodal data, while MMGN propagates multimodal messages in the video graph based on the adjacency matrix learned from histogram statistics of wireless data. Thanks to the robustness of the wireless data to visual noise and the collaboration of various modules, UMTF is capable of learning a model free of the human label on data. Extensive experimental results conducted on two challenging datasets, i.e., WP-ReID and DukeMTMC-VideoReID demonstrate the effectiveness of the proposed method.

Index Terms—Person re-identification, wireless positioning, unsupervised learning, multimodal.



1 INTRODUCTION

PERSON re-identification is essentially a person retrieval task in a multi-camera surveillance network. Given an image or video of a person that we are interested in, it aims to find out the images or videos of this person from a large data corpus captured by multiple surveillance cameras. The supervised person re-identification [1], [2], [3], [4], [5], [6], [7], [8] requires massive and exhaustive identity labeling of the cross-camera data, which is laborious and suffers the scalability issue in real-world applications. To bypass the label requirement, unsupervised person re-identification [9], [10], [11], [12], [13], [14], [15] is proposed to directly learn models from unlabeled data. Thanks to its favorable potential, it has received substantial attention from both academia and industry in recent years.

The existing unsupervised person re-identification methods rely on visual cues for model training. Although remarkable progress has been made, the defects of the visual data limit their further improvements. In other words, the occlusion and blur lead to the loss of distinguishing parts of pedestrians. Besides, the changes in viewpoints and clothing cause significant appearance changes in pedestrians. These visual noises can easily mislead existing methods that rely solely on visual clues. When the visual data is unreliable, the performance of these methods cannot be guaranteed. These defects of visual data force us to seek new supplementary information to increase the robustness of the system.

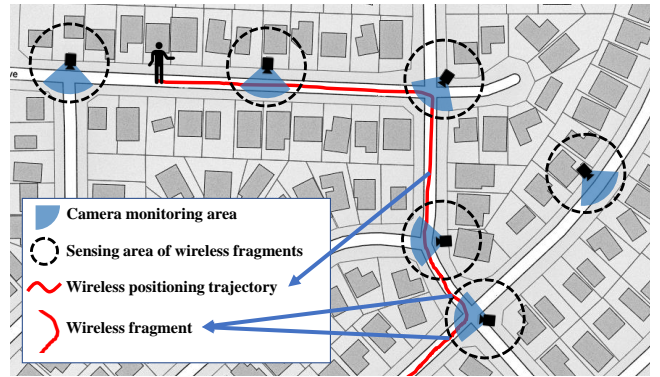


Fig. 1. The problem we study in this work. The wireless positioning trajectories of pedestrians carrying mobile phones can be obtained by existing cellular networks and WiFi positioning. Video data are captured when pedestrians walk to the monitoring areas of cameras. We consider the area within a preset sensing radius centered on the camera as the sensing area of the wireless trajectory fragments. When a pedestrian carrying a mobile phone enters the sensing area of the wireless fragments, the fragment of the wireless positioning trajectory within the sensing area is the sensed wireless fragment. The wireless fragment may belong to the same pedestrian as one of the videos captured by this camera during its time range.

For the person re-identification task, there have been some attempts to use the multimodal data. Fan *et al.* [16] propose to use radar signals for supervised person re-identification, but additional radar equipment is required. Liu *et al.* [17] introduce the wireless position trajectories for cross-domain person re-identification. Wireless positioning trajectories can be obtained through off-the-shelf

Yiheng Liu, Wengang Zhou, Qiaokang Xie, and Houqiang Li are with the CAS Key Laboratory of Technology in Geo-spatial Information Processing and Application System, Department of Electronic Engineering and Information Science, University of Science and Technology of China, Hefei, 230027, China. E-mail: {lyh156, xieqiaok}@mail.ustc.edu.cn, {zhwg, lihq}@ustc.edu.cn. Corresponding authors: Wengang Zhou and Houqiang Li.

equipment, such as cellular networks and WiFi positioning systems. The immutability of signal ID allows it to assist vision-based person re-identification task. However, they need to label the GPS coordinate of each location of the monitoring areas to map the pixel coordinate to the world coordinate for calculating the distance between videos and wireless signals [17]. Such a paradigm suffers the scalability issue since in real scenarios, labeling and maintaining the location information of each position in all monitoring areas extremely consumes human labor.

Based on the above discussion, as shown in Fig. 1, we propose a new setting to assist unsupervised person re-identification with wireless trajectories to mitigate the effects of visual noise (Fig. 2). For pedestrians carrying mobile phones, their wireless positioning trajectories can be obtained through existing cellular networks and WiFi positioning. We define the circular area whose distance from the surveillance camera is less than a preset distance as the wireless fragment sensing area of this camera. Once a pedestrian carrying a mobile phone enters this area, we assume that a person enters the monitored area and a wireless fragment is sensed. The wireless fragment is the fragment of the wireless positioning trajectory within the circular sensing area. The video of the owner of the wireless trajectory should belong to the set of videos captured by the corresponding camera during the time range of this wireless fragment. This weak relationship allows us to use wireless data to assist person re-identification. Different from [16], our setting does not require new equipment. Compared with [17] which assumes the GPS coordinate labeling on the entire monitoring areas, our weak scene labeling setting only needs to access the locations of cameras. Therefore, our setting is more feasible and scalable for large-scale surveillance scenarios than previous settings [16], [17].

Our weak scene labeling makes the monitoring system easier to maintain and deploy, but it also brings great challenges. In each surveillance scene, since many pedestrians are carrying mobile phones, multiple videos and multiple wireless fragments are captured simultaneously. For a wireless fragment, the video of its owner is mixed in the videos captured by the corresponding camera during its time range, but we don't know which video corresponds to, since the association between videos and wireless fragments is unknown. This weak physical connection brings great challenges for us to use it to assist person re-identification.

In this work, we propose a new task, which is to use wireless positioning trajectories to assist unsupervised person re-identification under weak scene labeling. To handle the challenges in this new task, we devise a novel unsupervised multimodal training framework (UMTF), which contains a multimodal data association strategy (MMDA) and a multimodal graph neural network (MMGN). MMDA constructs detailed multimodal data associations through an adaptive clustering method. MMGN passes multimodal messages in the video graph by adaptively learning the adjacency matrix from multimodal data. By using these modules to mine the potential clues in unlabeled multimodal data, UMTF improves the model quality progressively. The experimental results conducted on two challenging datasets, *i.e.* WP-ReID and DukeMTMC-VideoReID, demonstrate the effectiveness of our method.

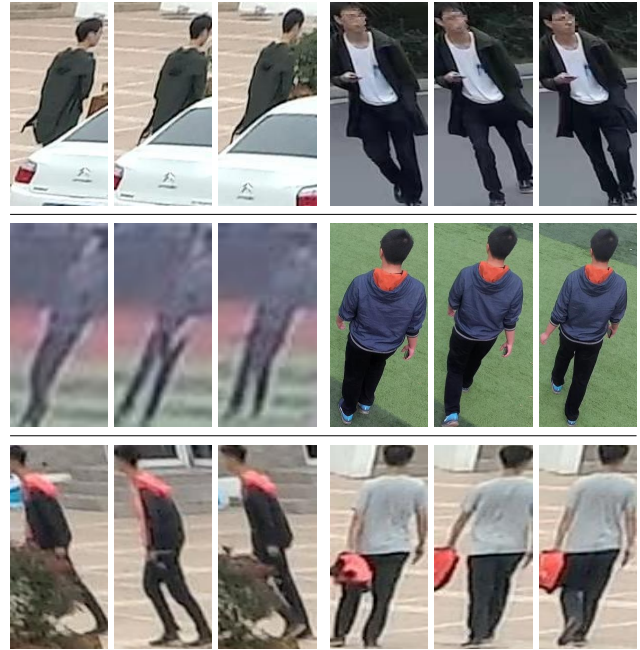


Fig. 2. The occlusion, blur and clothing changes examples on existing person re-identification datasets, which introduce many challenges for existing methods that rely on visual data. Each row in the figure contains two video sequences belonging to the same person, each with three frames.

2 RELATED WORKS

In this section, we first briefly review the progress of supervised and unsupervised person re-identification. Then we introduce some research efforts with multimodal data to assist vision tasks, especially person re-identification.

2.1 Person Re-identification

Supervised Person Re-Identification. To solve the difficulties caused by occlusion, blur, dramatic variations of pedestrian's postures and viewpoints, a lot of work are devoted to designing better models to extract distinguishable and robust visual feature representation. According to the type of data processed, these methods can be divided into image-based methods [18], [19], [20], [21], [22], [23] and video-based methods [24], [25], [26], [27], [28], [29].

For image-based person re-identification, in [30], a part-aligned representation model is proposed to handle the body misalignment problem. The human body is decomposed into regions that are weighted with the part maps generated by a part net. In [18], a multi-scale deep learning model is designed to learn multi-scale discriminative feature representations and a saliency-based learning fusion layer is used to automatically determine the most suitable scales for matching. In [20], HydraPlus-Net is proposed to capture multiple attentions from low-level to semantic-level and extract the multi-scale attention-strengthened features. Liu *et al.* [23] use both person ID and camera ID to train a model to decouple features into the foreground and background features.

Video-based person re-identification [25], [26], [31], [32], [33] mainly focuses on integrating temporal information.

McLaughlin *et al.* [31] introduce a recurrent neural network to fuse the temporal features extracted from each frame. Chung *et al.* [25] use a siamese network to extract features from the original video frames and optical flow images, respectively. The motion information contained in the optical flow is integrated into the final features. Liu *et al.* [26] design a recurrent refining unit to integrate appearance representations and motion information to suppress the noise in the videos and refine the features. In [27], [28], different kinds of attention networks are designed to fuse the features of video frames.

Unsupervised Person Re-Identification. To reduce the cost of manual labeling and increase the scalability in real scenarios, unsupervised person re-identification aims to train a discriminative model on unlabeled person re-identification datasets. Due to the lack of training labels, how to mine the potential relationships among data is the key to this task. As a representative solution, Li *et al.* [34] propose an unsupervised tracklet association learning (UTAL) model to automatically eliminate the pedestrian ID labeling. Through the per-camera tracklet discrimination learning and cross-camera tracklet association learning, UTAL model achieves good pedestrian distinguishing capability. Chen *et al.* [35] jointly optimize two margin-based association losses to constrain the association of each frame and automatically discover the more reliable cross-camera tracklets. In [36], [37], the dynamic graph matching (DGM) method is used to iteratively update the data graph and the label estimation process. With the intermediate estimated labels, the model can learn a better feature representation. Xie *et al.* [38] introduce the spatio-temporal constraint to promote the label generation. Lin *et al.* [39] introduce several auxiliary information as additional priors for constraints, including a camera-based term that is useful for distance amendment.

2.2 Multimodal Data and Vision Tasks

Since visual data is easily affected by blur, occlusion, and background clutter, *etc.*, seeking multimodal data to make up for the defects of visual data has become an emerging research direction. To this end, some settings [40], [41], [42], [43], [44] have been explored with promising results.

WiFi Signals and Vision Tasks. In [40], [41], the wireless signal strength is used to assist visual tracking tasks. But the change of signal strength is very susceptible to the influence of the environment, which makes their method unreliable. Korany *et al.* [42] extract gait information from the CSI magnitude measurement of WiFi for person identification, which requires a high quality of visual data to facilitate the human 3D mesh extraction.

WiFi Sniffing and Face Recognition. In [43], [44], WiFi sniffing is adopted to sense the wireless signal of a person's mobile device for face recognition. However, for privacy protection, the current mobile phone system returns random MAC addresses for WiFi sniffing, which does not support the assumption of this approach. Meanwhile, these methods need to divide the data into different events such as meals, meetings, and fitness according to time and location. Since the person re-identification task is uninterrupted and the content is consistent, this strategy does not apply to person re-identification.

Multimodal Data and Person Re-Identification. There are also some efforts [16], [17] to explore the use of multimodal data on person re-identification. Fan *et al.* [16] utilize radar signals for person re-identification without considering visual data. Liu *et al.* [17] introduce the wireless positioning trajectories of mobile devices to assist cross-domain person re-identification. To measure the distance between the videos and the wireless trajectories, this method needs to manually label the GPS coordinate of each location under each camera scene to map the pixel coordinate to the world coordinate. However, it is laborious to label and maintain the coordinates of all positions, which limits their application in large-scale surveillance scenarios.

Privacy Protection of Wireless Data. Wireless positioning data are important private data for pedestrians. When using wireless positioning data to assist vision tasks, it is unavoidable to consider privacy protection. Fortunately, cellular network positioning is provided by the mobile communication company, which makes the positioning information easy to be protected and regulated by relevant organizations to avoid misuse and leakage of data. For the positioning method via WiFi, pedestrians can avoid the leakage of location information by connecting to a trusted router. Therefore, the use of wireless positioning data is controllable and reliable in terms of privacy protection.

3 OUR METHOD

Fig. 3 shows the overall workflow of our proposed unsupervised multimodal training framework (UMTF), which mainly includes two training stages. The first stage performs intra-camera model learning to obtain a model $F(\cdot)$ with basic pedestrian discrimination capability. In the second training stage, $F(\cdot)$ and the multimodal graph neural network (MMGN) generate pseudo visual labels and pseudo multimodal labels to guide each other's training. In the following subsections, after introducing our problem formulation, we will elaborate UMTF from three aspects: the generation of pseudo visual labels, the generation of pseudo multimodal labels, and the mutual promotion of the dual models.

3.1 Problem Formulation

In Fig. 3, the input of UMTF contains two kinds of data, *i.e.* the video sequences $\{\mathbf{V}_i\}_{i=1}^N$ captured by C cameras and the wireless positioning trajectories $\{\mathbf{T}_m\}_{m=1}^M$. N is the number of video sequences, C is the total number of cameras, and M is the number of wireless trajectories. Under the setting of our weak scene labeling, we know the location of each camera. As shown in Fig. 1, for each camera, a circular area with a preset radius around it is considered as its wireless sensing area. The part of the wireless trajectory \mathbf{T}_m located inside the circular wireless fragment sensing area is treated as a wireless fragment \mathbf{T}_m^r . Every time the owner of the wireless trajectory passes through a monitoring area, a wireless fragment is sensed. $\{\mathbf{T}_m^r\}_{r=1}^{R_m}$ denotes R_m wireless fragments belonging to wireless trajectory \mathbf{T}_m and they share the same signal ID, such as MAC address.

The features of video sequences $\{\mathbf{V}_i\}_{i=1}^N$ are fine-grained descriptions of the appearance of pedestrians but are sensitive to visual noise. Meanwhile, it is unknown which video

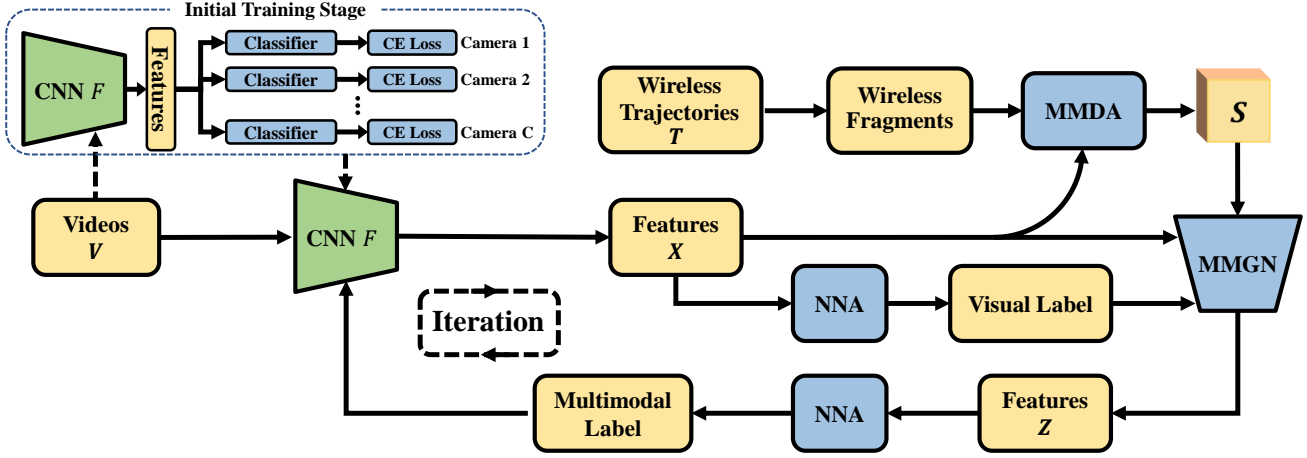


Fig. 3. The overall workflow of our unsupervised multimodal training framework (UMTF). NNA is the nearest neighbor association. MMDA is the multimodal data association strategy. MMGN means the multimodal graph neural network. The CNN model obtained from the initial training stage is sent to the second training stage to be alternately trained with MMGN. The CNN model and MMGN generate pseudo visual labels and pseudo multimodal labels to guide and promote each other in the multiple iterations and updates.

TABLE 1
The definition of different mathematical notations in our method.

Variable	Definition
\mathbf{V}_i	The i^{th} video sequence.
\mathbf{T}_m	The m^{th} wireless positioning trajectory.
\mathbf{T}_m^r	The r^{th} wireless fragment of \mathbf{T}_m .
R_m	The total number of wireless fragments belonging to \mathbf{T}_m .
\mathcal{V}_m^r	The video set related to \mathbf{T}_m^r .
$\mathcal{C}_{m,k}$	The k^{th} cluster.
K_m	The number of clusters of videos related to \mathbf{T}_m .
$\mathbf{P}_{m,k}$	The probability of cluster $\mathcal{C}_{m,k}$ belonging to \mathbf{T}_m .
$\mathbf{S}_{i,j,m}$	The wireless similarity measurement between \mathbf{V}_i and \mathbf{V}_j under m^{th} wireless trajectory.
\mathbf{A}^{avg}	The average result of the wireless channel of \mathbf{S} .
\mathbf{S}^h	The histogram of the wireless channel of \mathbf{S} .
\mathbf{A}	The final adjacency matrix of video graph.

sequences belong to the same person. The wireless trajectories $\{\mathbf{T}_m\}_{m=1}^M$ are very reliable, but only roughly describe the movement of pedestrians. The associations between video sequences and wireless fragments are also unknown. We don't know which video sequence and which wireless fragment belong to the same person. In our proposed new task, *i.e.* unsupervised person re-identification with wireless positioning under weak scene labeling, we only label the locations of cameras. The goal of this task is to train a high-performance person re-identification model $F(\cdot)$ using unlabeled visual data and unlabeled wireless positioning trajectories when knowing the locations of cameras.

3.2 Generation of Pseudo Visual Labels

Initial Training Stage. To obtain the pseudo visual labels, we need an initial model with basic pedestrian discrimination capability. As shown in the initial training stage of Fig. 3, we use a multi-branch network architecture [34], [38] to train the basic model. The network has a shared feature extraction model $F(\cdot)$ and C independent classifiers. Given a video sequence \mathbf{V}_i , the model $F(\cdot)$ extracts the feature of

each frame and averages them to get the video-level feature $\mathbf{x}_i \in \mathbb{R}^{2048}$. The features of the video sequences from each of C cameras are fed to the corresponding classifier. For each classifier, the number of classes is equal to the number of video sequences captured by the corresponding camera, *i.e.* every video sequence is treated as an independent class. We use the cross-entropy loss to train each classifier. The total loss is the sum of the C cross-entropy losses.

Nearest Neighbor Association. After the initial training stage, we obtain a model $F(\cdot)$ with basic pedestrian discrimination capability. Given N video sequences, we extract their features with $F(\cdot)$. Then, we apply the nearest neighbor association (NNA) [34], [38] for cross-camera video sequences association and obtain the pseudo visual labels. Specifically, for each video sequence, NNA first finds cross-camera nearest neighbor on each camera pair based on the cosine similarity of the features. Then, for two video sequences, if they are the cross-camera nearest neighbor of each other, they are regarded as belonging to the same person and assigned the same pseudo visual label. Since being the cross-camera nearest neighbors to each other is a strong constraint, not all video sequences are assigned pseudo visual labels. During the training process, we filter out these unlabeled video sequences, but this does not affect the design of the algorithm. Therefore, in the following narration, we assume that all video sequences are assigned pseudo visual labels for brevity.

3.3 Generation of Pseudo Multimodal Labels

The generation of pseudo multimodal labels relies on two main modules, *i.e.*, multimodal data association strategy (MMDA) and multimodal graph neural network (MMGN). MMDA associates visual data and wireless data with the adaptive clustering method. Different from GCN [45] and GAT [46], MMGN adaptively learns the adjacency matrix from the histogram statistics of wireless similarity.

Multimodal Data Association. In the setting of [17], since the latitude and longitude of each location in scenes

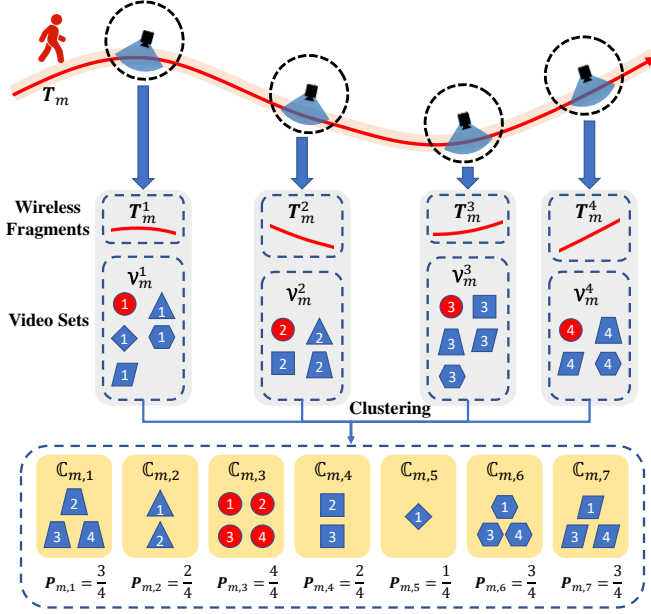


Fig. 4. The process of multimodal data association (MMDA). The circular area (the area inside the dotted circle) with a preset radius around each camera is regarded as the wireless fragment sensing area. The part of a pedestrian's wireless positioning trajectory T_m located in a wireless sensing area is regarded as a wireless fragment T_m^r . In this example, 4 wireless fragments $\{T_m^r\}_{r=1}^4$ are sensed when the pedestrian pass by 4 surveillance cameras. We use different markers to represent video sequences. Video sequences with the same marker share the same person identity. The number in a marker is the serial number of the corresponding wireless fragment. Taking T_m^1 as an example, during the time range of T_m^1 , 5 video sequences of pedestrians are captured by the corresponding camera, which are denoted as a video set V_m^1 . The video sequence (red circle) of the target pedestrian is mixed in the video set V_m^1 . MMDA is dedicated to correctly associating the wireless trajectory of the target person with its video sequences (red circles).

captured by cameras is labeled, the visual data and wireless data are directly correlated by measuring the distance between the visual trajectories and the wireless trajectories. However, in our task, we adopt the weak scene labeling. We only need to know the locations of cameras, not the latitude and longitude of each location of the scenes captured by the cameras. This reduces the cost of scene annotation, but it also brings great challenges to the association and fusion of multimodal data. To this end, we design a multimodal data association strategy (MMDA), which divides the visual data and wireless data in time and space based on the locations of cameras, and then mine the correlation between them.

As shown in Fig. 4, a circular area (the area inside the dotted circle) with a preset radius around a surveillance camera is defined as the sensing area for wireless fragments. For a target pedestrian carrying a mobile phone, we can obtain the wireless positioning trajectory T_m by cellular networks or WiFi positioning. The part of the wireless trajectory T_m located in a wireless sensing area is the sensed wireless fragment T_m^r . We use different markers to represent video sequences. Video sequences with the same marker share the same person identity. The number in a marker is the serial number of the corresponding wireless fragment. During the time range of the wireless fragment T_m^1 , if there is only the target pedestrian in the surveillance area, the video

sequences captured by the camera at this time belongs to the same person as the wireless fragment. However, many pedestrians often appear in the monitoring scene at the same time. In this case, the video sequence (red circle) of the target person is mixed with a bunch of video sequences V_m^1 captured by the corresponding camera during the time range of this wireless fragment T_m^1 . We use V_m^r to represent these video sequences related to wireless fragment T_m^r .

In Fig. 4, given multiple wireless fragments $\{T_m^r\}_{r=1}^4$, we obtain corresponding related video sets $\{V_m^r\}_{r=1}^4$. The video sequences (red circles) belonging to the target pedestrian are mixed with these video sets. The goal of MMDA is to accurately estimate the probability that each video sequence in $\{V_m^r\}_{r=1}^4$ belongs to the same person as this wireless trajectory T_m .

Since the person re-identification model $F(\cdot)$ has a certain capability to distinguish pedestrians, we use $F(\cdot)$ to extract the features of the video sequences in $\{V_m^r\}_{r=1}^4$. As shown in Fig. 4, we apply the k -means clustering algorithm on the features and get K_m clusters $\{C_{m,k}\}_{k=1}^{K_m}$. The value of K_m , i.e., the number of the clusters is estimated adaptively, which will be described in a later paragraph. Video sequences belonging to the same pedestrian are similar and their features are likely to be clustered together. Therefore, we assume that the video sequences in the same cluster belong to the same person. This assumption introduces some noise because the clustering results are not always accurate. However, our experimental results show that with the increase of training epochs, the clustering results will get better and better and achieve satisfactory results. This assumption can still assist multimodal data association well.

Since a wireless fragment T_m^r is sensed when wireless trajectory T_m passes through a monitoring area. As illustrated in Fig. 4, T_m has $R_m = 4$ wireless fragments $\{T_m^r\}_{r=1}^{R_m=4}$ because it passes through 4 monitoring areas. Therefore, the owner of this wireless trajectory should have passed through these four monitoring areas as well. This indicates that we can use the consistency of the motion path of the pedestrian represented by the video sequences contained in the cluster $C_{m,k}$ and the path of the wireless trajectory T_m to measure the possibility that they belong to the same person.

For each video sequence, we know which camera it is captured by. So for the pedestrian represented by video cluster $C_{m,k}$, we can easily obtain the number of monitoring scenes it passes through. We define function $Q(C_{m,k})$ to return this number. Taking the clustering results in Fig. 4 as an example, the video sequences contained in the cluster $C_{m,7}$ are from the video sets V_m^1, V_m^3 and V_m^4 . Therefore, $Q(C_{m,7}) = 3$. This indicates that the pedestrians represented by $C_{m,7}$ passed through three of the $R_m = 4$ monitoring areas that the wireless trajectory T_m passed through. Their paths are not perfectly matched. To measure the probability that the video cluster $C_{m,k}$ and the wireless trajectory T_m belong to the same person, we define the consistency between the pedestrian's motion path represented by the video cluster $C_{m,k}$ and that of the wireless trajectory T_m as

$$P_{m,k} = \frac{Q(C_{m,k})}{R_m}. \quad (1)$$

The closer $\mathbf{P}_{m,k}$ is to 1, the more consistent the path of the pedestrian represented by cluster $\mathcal{C}_{m,k}$ is with the path of the wireless trajectory \mathbf{T}_m , and the more likely they are to belong to the same person.

For the cluster $\mathcal{C}_{m,3}$ in Fig. 4, $Q(\mathcal{C}_{m,3}) = 4$. The pedestrian represented by it passes through all $R_m = 4$ monitoring areas where the wireless trajectory \mathbf{T}_m passes, so $\mathbf{P}_{m,3} = \frac{Q(\mathcal{C}_{m,3})}{R_m} = \frac{4}{4} = 1$, which indicates that the video sequences in this cluster are likely to belong to the same person as the wireless trajectory \mathbf{T}_m . So far, through the processing of MMDA shown in Fig. 4, we obtain the association between the visual data and the wireless trajectory \mathbf{T}_m . By repeating this process for all wireless trajectories, we can obtain the association between the visual data and all wireless data.

Adaptive estimation of the number of clustering centers. In the above process of obtaining associations between video sequences and the wireless trajectory \mathbf{T}_m , we need to apply k -means algorithm on video sets $\{\mathcal{V}_m^r\}_{r=1}^{R_m}$. Instead of using a manually preset K_m for the number of clustering centers, we design a method to automatically estimate the appropriate number for K_m .

Generally, every time a pedestrian passes through a monitoring scene of a camera, a video sequence and a wireless fragment are sensed. Therefore, the average number of wireless fragments of a trajectory can roughly reflect the average number of video sequences belonging to a person, which can be calculated as $\frac{\sum_{m=1}^M R_m}{M}$. R_m is the number of wireless fragments belonging to m^{th} wireless trajectory \mathbf{T}_m . $\sum_{m=1}^M R_m$ is the total number of wireless fragments of all wireless trajectories. M is the total number of wireless trajectories. R_m and M are known values that do not require human labeling. $\frac{\sum_{m=1}^M R_m}{M}$ reflects the average number of wireless fragments a wireless trajectory (pedestrian) has, and is also an appropriate estimate of the average number of video sequences a pedestrian has.

For wireless trajectory \mathbf{T}_m , the video sequences in video sets $\{\mathcal{V}_m^r\}_{r=1}^{R_m}$ are related to it. The total number of these video sequences related to \mathbf{T}_m is $\sum_{r=1}^{R_m} |\mathcal{V}_m^r|$. Since we have estimated that the average number of video sequences a pedestrian has is $\frac{\sum_{m=1}^M R_m}{M}$. Then, we can estimate that these video sequences related to wireless trajectory \mathbf{T}_m come from $\frac{\sum_{r=1}^{R_m} |\mathcal{V}_m^r| \times M}{\sum_{m=1}^M R_m}$ pedestrians.

Considering the purpose of clustering is to gather videos belonging to the same person into one cluster, $\frac{\sum_{r=1}^{R_m} |\mathcal{V}_m^r| \times M}{\sum_{m=1}^M R_m}$ is a good estimate for the number of clustering centers K_m . However, in a real situation, a pedestrian passing through a monitoring scene may have intermittent tracking videos due to occlusion, which makes the pedestrian has one wireless fragment but be captured in multiple video sequences in this scene. This makes the number of wireless fragments a person owns not a completely accurate reflection of the number of video sequences a person owns. Besides, the walking routes of pedestrians are different, which makes the estimated person number deviating from the true person number. Considering the above cases, we amend the

estimation formula of K_m as

$$K_m = \lambda \frac{\sum_{r=1}^{R_m} |\mathcal{V}_m^r| \times M}{\sum_{m=1}^M R_m}, \quad (2)$$

where coefficient λ controls the proportional relationship between K_m and the estimated number of pedestrians. By roughly adjusting λ to an appropriate value, K_m can approach the true person number very well. Instead of manually selecting the same number K for all wireless trajectories without clues, our method can adaptively calculate the appropriate number of clusters for videos released to different trajectories.

It is worth emphasizing that the above strategy for estimating the number of clustering centers does not break the unsupervised task setting. Each wireless trajectory has a unique identification, *e.g.*, MAC address, so we can directly obtain the number of wireless trajectories without manual labeling. wireless fragments are obtained directly by judging the distance between the wireless trajectories and cameras, which are also free of manual labeling. The videos $\{\mathcal{V}_m^r\}_{r=1}^{R_m}$ related to a pedestrian's wireless trajectory \mathbf{T}_m are a small fraction of the videos captured by the entire surveillance network. We cannot know exactly how many pedestrians these videos are from without manually labeling. Therefore, we roughly estimate it by estimating the number of video sequences a pedestrian has. This estimated number, although not completely accurate, is an appropriate reference for the number of clustering centers.

Wireless Similarity. Although we obtain the association between visual data and wireless data by MMDA shown in Fig. 4, the association results of the multimodal data need to be further processed to be used in the training of person re-identification models. For two video sequences in the cluster $\mathcal{C}_{m,k}$, when $\mathbf{P}_{m,k}$ is large, both of them are likely to belong to one pedestrian. This means that the two video sequences should be very similar, which suggests that we can take this value as the similarity of the two videos based on wireless data. With such consideration, we define a similarity measurement strategy between \mathbf{V}_i and \mathbf{V}_j based on m^{th} wireless trajectory as

$$\mathbf{S}_{i,j,m} = \begin{cases} \mathbf{P}_{m,k} & \text{if } i \neq j \text{ and } \exists \mathcal{C}_{m,k}, \{\mathbf{V}_i, \mathbf{V}_j\} \subseteq \mathcal{C}_{m,k}, \\ 1 & \text{if } i = j, \\ 0 & \text{otherwise,} \end{cases} \quad (3)$$

where $\mathbf{S} \in \mathbb{R}^{N \times N \times M}$ and $\mathbf{S}_m \in \mathbb{R}^{N \times N}$ embodies the similarities between the N videos based on the m^{th} wireless trajectory \mathbf{T}_m . During the data association process of MMDA, only video sequences with temporal and spatial overlap with the wireless fragments are related to a corresponding wireless trajectory, which results in \mathbf{S}_m being a sparse matrix.

Multimodal Graph Neural Network. Through the process described above, we get a new wireless similarity measurement \mathbf{S} between video sequences. To make better use of it, we build a video graph containing N nodes. Each node denotes a video sequence and is described by the feature \mathbf{x}_i obtained from model $F(\cdot)$. After defining the nodes, one way to construct the adjacency matrix is to directly take the mean value of \mathbf{S} along the third dimension as the adjacency matrix \mathbf{A}^{avg} , where $\mathbf{A}_{i,j}^{\text{avg}} = \sum_m \mathbf{S}_{i,j,m} / M$. With features

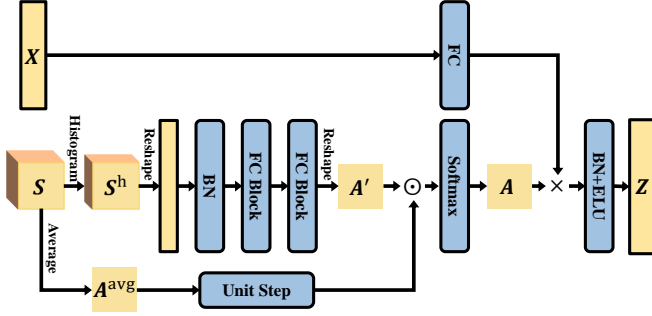


Fig. 5. The architecture of the multimodal graph convolutional module (MGM). $\mathbf{S} \in \mathbb{R}^{N \times N \times M}$ are the wireless similarity between N videos. $\mathbf{X} \in \mathbb{R}^{N \times 2048}$ are the features of N video sequences. The output features $\mathbf{Z} \in \mathbb{R}^{N \times 512}$ are the video features updated with wireless information. \odot denotes the element-wise multiplication. \times is the matrix multiplication.

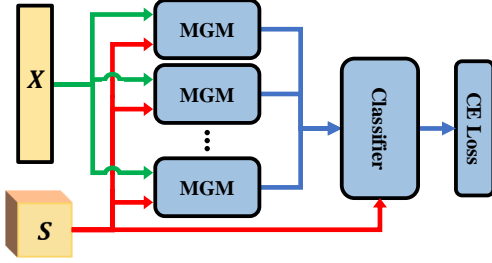


Fig. 6. The overall architecture of the multimodal graph neural network (MMGN). MGM denotes the multimodal graph convolutional module. $\mathbf{S} \in \mathbb{R}^{N \times N \times M}$ are the wireless similarity between N videos. $\mathbf{X} \in \mathbb{R}^{N \times 2048}$ are the features of N video sequences.

$\mathbf{X} \in \mathbb{R}^{N \times 2048}$ and the adjacency matrix $\mathbf{A}^{\text{avg}} \in \mathbb{R}^{N \times N}$, we can use the graph convolutional network (GCN) [45] to pass message. However, \mathbf{A}^{avg} is obtained by directly averaging the wireless channel of the sparse matrix \mathbf{S} , which will cause oversmoothing if M is very large. Besides, the averaging of the wireless channel loses the distribution information of wireless similarity under different wireless trajectories.

Based on the above considerations, we propose a multimodal graph convolutional module (MGM) to make better use of the information provided by wireless similarity \mathbf{S} . As shown in Fig. 5, given \mathbf{S} , we first count its histogram $\mathbf{S}^h \in \mathbb{R}^{N \times N \times 32}$, which is formulated as

$$\mathbf{S}_{i,j}^h = \frac{h(\mathbf{S}_{i,j})}{M}, \quad (4)$$

where $h(\cdot)$ divides the $[0, 1]$ into 32 bins with equal size and returns the histogram of the input. $\mathbf{S}_{i,j}^h$ uses 32 bins to reflect the distribution in wireless similarity $\mathbf{S}_{i,j} \in \mathbb{R}^M$ between \mathbf{V}_i and \mathbf{V}_j on multiple wireless trajectories. Given the histogram distribution \mathbf{S}^h of wireless similarity \mathbf{S} , we further use several neural network layers to adaptively learn the adjacency matrix $\mathbf{A} \in \mathbb{R}^{N \times N}$ of the graph.

As shown in Fig. 5, \mathbf{S}^h is first reshaped to a 2D matrix with shape $\mathbb{R}^{N \times 32}$ and each 32-dim vector is treated as a feature vector. Then, the result is fed to two FC blocks to get $\mathbf{A}' \in \mathbb{R}^{N \times N}$. Each block contains a fully connected layer (FC), a batch normalization (BN) layer and a leaky rectified linear unit. These two FC blocks output 16-dim and

1-dim features, respectively. Finally, we get the adjacency matrix \mathbf{A} by $\mathbf{A} = \text{softmax}(\mathbf{A}' \odot u(\mathbf{A}^{\text{avg}}))$, where $u(\cdot)$ is the unit step function. $u(\cdot) = 1$ when the input value is larger than 0, otherwise $u(\cdot) = 0$. \odot denotes the element-wise multiplication. $\mathbf{A}' \odot u(\mathbf{A}^{\text{avg}})$ filters out the learned association between two video sequences in \mathbf{A}' that have no wireless-based association. The softmax operation is to normalize each row of the matrix.

Different from GAT [46] that learns the adjacency matrix from pairs of video features, our adjacency matrix \mathbf{A} is learned from the wireless similarity that contains multimodal information with our carefully designed network structure. Meanwhile, compared with the adjacency matrix \mathbf{A}^{avg} obtained by the averaging operation, \mathbf{A} makes better use of the wireless similarity and adapts to this graph.

After obtaining the learned adjacency matrix \mathbf{A} , we first embed the features $\mathbf{X} \in \mathbb{R}^{N \times 2048}$ of N video sequences into 512-dim features by a FC layer. Then, by multiplying \mathbf{A} , we get the video features after message passing. Finally, we get the final video features $\mathbf{Z} \in \mathbb{R}^{N \times 512}$ after the processing of BN and exponential linear unit (ELU). As shown in Fig. 5, \mathbf{Z} is the video feature representation after updating the raw video features \mathbf{X} with the wireless similarity \mathbf{S} between videos. Since \mathbf{Z} considers both visual and wireless data, it can also be called the multimodal feature representation of video sequences.

With the designed MGM, as shown in Fig. 6, we further propose a multimodal graph neural network (MMGN) to strengthen the use of multimodal data. To enhance the representation capability of features, similar to [46], [47], we use the multi-head mechanism to concatenate features generated by 6 MGMs to achieve the final representation. The classifier is also a MGM module, while the final BN layer and ELU layer are removed and the dimension of the output is the number of classes.

3.4 The Mutual Promotion of the Dual Models

In our proposed unsupervised multimodal training framework (UMTF), different modules cooperate to get better results progressively. As shown in Fig. 3, in the initial training stage, we obtain a model $F(\cdot)$ with basic pedestrian discrimination capability. In the second training stage, model $F(\cdot)$ extracts the visual feature representation $\mathbf{X} \in \mathbb{R}^{N \times 2048}$. With \mathbf{X} , as described in Section 3.2, we use the nearest neighbor association (NNA) to generate pseudo visual labels.

On the video graph, MMGN learns the adjacency matrix adaptively from the histogram distribution of wireless similarity \mathbf{S} with the specially designed multimodal graph convolutional modules (MGM). The input of MMGN is the raw videos features \mathbf{X} . The output of MMGN is video features mixed with wireless information, *i.e.*, the multimodal features $\mathbf{Z} \in \mathbb{R}^{N \times 512}$ of video sequences. MMGN is trained by cross-entropy loss with pseudo visual labels.

With the trained MMGN, we update \mathbf{X} and get updated multimodal features $\mathbf{Z} \in \mathbb{R}^{N \times 512}$. Similar to the process described in Section 3.2, we apply the nearest neighbor association (NNA) on \mathbf{Z} to obtain the pseudo multimodal labels, which can be adopted for the further training of model $F(\cdot)$ with the batch hard triplet loss [48].

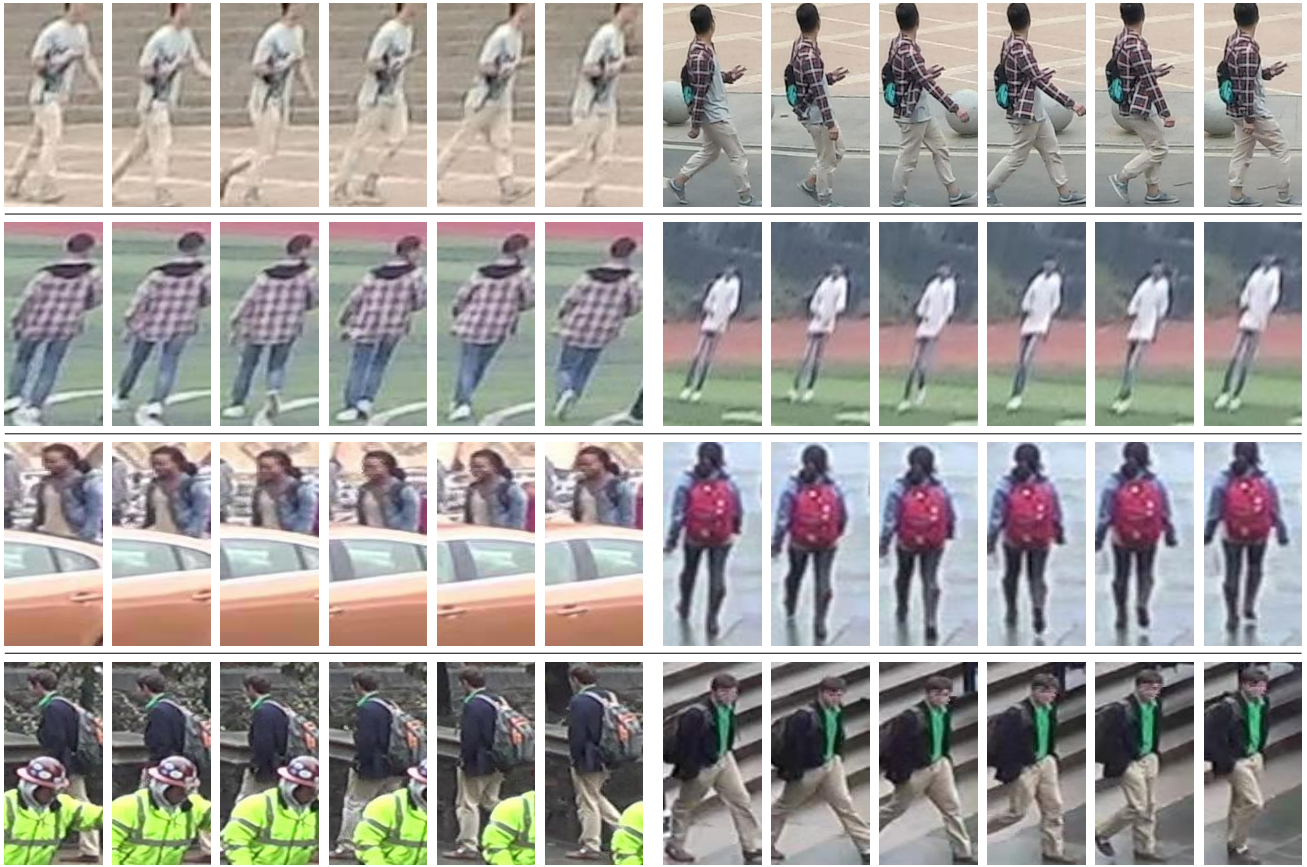


Fig. 7. Examples of the matching results of our method. Each row in the figure contains two videos belonging to the same person, each with six frames. The first two rows of videos are from WP-ReID dataset, and the videos in the next two rows are from DukeMTMC-VideoReID. These videos are difficult to match correctly by existing vision-based methods because of clothes changing, blur and occlusion issues. Thanks to the reliability of the wireless signals, our method avoids the interference of visual factors and matches them correctly.

In summary, as illustrated in Fig. 3, the training of $F(\cdot)$ and MMGN are performed alternately. With the pseudo labels provided by the other model, they are trained again to obtain better models and estimate more accurate pseudo labels for the other model. In such multiple iterations, they progressively promote each other and reach a stable state. Finally, we obtain a more discriminative model $F(\cdot)$ for inference.

4 EXPERIMENT

4.1 Experimental Setup

Datasets. We evaluate our proposed method on two person re-identification datasets, *i.e.* WP-ReID [17] and DukeMTMC-VideoReID [49]. WP-ReID [17] contains both video sequences and authentic wireless positioning trajectories of the mobile phones carried by pedestrians. In WP-ReID, 868 video sequences of 79 pedestrians are captured by six cameras. Among them, 29 pedestrians have corresponding wireless trajectories. The captured scenes of three cameras overlap. Occlusion, blur, and clothing changes are common in this dataset. These factors make WP-ReID very challenging.

DukeMTMC-VideoReID [49] is a large person re-identification dataset containing only video data. 4,832 video sequences from 1,812 identities are captured by 8

cameras. Although this dataset has no wireless data, we can generate simulated wireless data that is very close to the real situation. We randomly select 80% pedestrians and assume that they carry mobile phones and can be collected wireless trajectories. For each video sequence \mathbf{V}_i of these people, we can generate a corresponding wireless fragment based on its timestamp. Considering the sensing range of the wireless data is usually larger than the monitoring area of the camera, the time range of the wireless fragment should be larger than the time range of the video sequence. Therefore, we add extra 15 seconds to the beginning and end of the time of the generated wireless fragment to extend the time range by 30 seconds.

The generation of simulated wireless data relies on the timestamp of each frame of the video sequence in the dataset. In the existing popular video-based large-scale person re-identification dataset, only DukeMTMC-VideoReID provides timestamps. Therefore, we generate simulated wireless data on DukeMTMC-VideoReID dataset only. DukeMTMC-VideoReID is a large-scale dataset with complex background and varied pedestrians, which makes it very challenging. The combination of WP-ReID dataset [17] with authentic wireless data and the large-scale DukeMTMC-VideoReID dataset [49] with simulated wireless data allows to fully validate the effectiveness of the

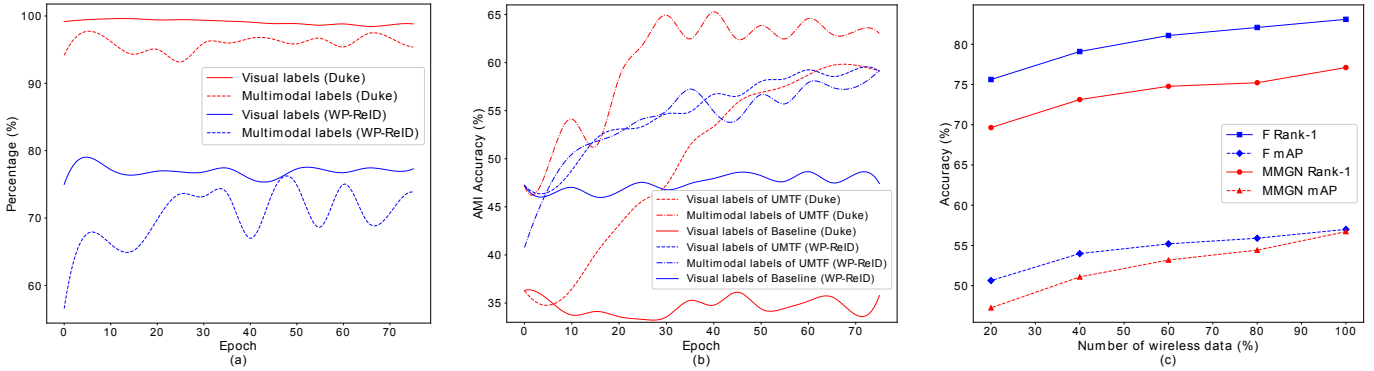


Fig. 8. (a) The number of video sequences assigned pseudo visual labels or pseudo multimodal labels as a percentage of the total number of videos. (b) The prediction accuracies of pseudo labels, which takes adjusted mutual information (AMI) as the evaluation metric. (c) The impact of the number of wireless signals on the performance of model $F(\cdot)$ and MMGN on WP-ReID dataset. We use Duke to denote the DukeMTMC-VideoReID dataset for brevity.

different methods.

Evaluation Protocols. WP-ReID [17] only provides test set. Following [17], we directly train the unsupervised model on the test set without any label. For DukeMTMC-VideoReID [49], we adopt the standard training and testing split, while the labels of the training set are not used. We take the standard Cumulated Matching Characteristics (CMC) table and mean Average Precision (mAP) as the evaluation metric of the two datasets. For CMC table, the scores at rank 1, 5, 10, 20 are reported. Rank- r visualizes an expectation of finding the correct person in the top r matches. To evaluate the performance of pseudo-label prediction or clustering, we use adjusted mutual information (AMI) as the evaluation metric, which measures the consistency between the obtained results and the ground truth labels.

Implementation Details. We take ResNet50 [50] pre-trained on ImageNet as the backbone model. The final FC layer is removed. The input frames are resized to 256×128 and the number of video frames is 8. For the initial training stage, we update the model for 80 epochs by the Adam algorithm with an initial learning rate of 3×10^{-4} . 128 video sequences are randomly selected for each training batch. In the second training stage, we re-estimate the pseudo labels every 5 epochs. For the training of model $F(\cdot)$ in the second stage, we update the model for 80 epochs by the SGD algorithm with a learning rate of 6×10^{-5} . Random horizontal flipping is adopted for data augmentation. We select video sequences of 32 pedestrians each with 4 video sequences as the inputs. The margin of the triplet loss is 0.4. When training MMGN, the network is updated for 80 epochs by the Adam algorithm with a learning rate of 0.01. The weight decay for all model training is set to 5×10^{-4} . For WP-ReID and DukeMTMC-VideoReID, λ is set to 3 and 2 by default, respectively. The sensing radius of wireless trajectories in WP-ReID dataset is 40 meters by default. **The code will be made publicly available.**

4.2 Ablation Study

As shown in Table 2, *Initial Training* directly uses the model obtained after the initial training stage for inference. *Baseline* uses the pseudo visual labels obtained through visual data for CNN model training in the second stage. MMDA and

TABLE 2

The ablation study of UMTF. *BL* denotes the baseline method, which directly train the model $F(\cdot)$ with the pseudo visual labels. Duke denotes the DukeMTMC-VideoReID dataset. MMGN^{G_{CN}} and MMGN^{G_{AT}} use GCN [45] and GAT [46] to replace the default MGM in MMGN. When MMGN is adopted, MMDA will also be adopted to provide wireless similarity.

Method	WP-ReID		Duke	
	mAP	Rank-1	mAP	Rank-1
Initial Training	26.3	66.7	67.6	75.1
Baseline	43.1	72.1	71.4	77.9
BL + MMGN ^{G_{CN}} [45]	48.2	75.6	74.6	80.8
BL + MMGN ^{G_{AT}} [46]	45.6	76.6	74.5	80.8
BL + MMGN (UMTF)	57.0	83.1	79.7	84.9

MMGN are not adopted in *Baseline*. Neither *Initial Training* nor *Baseline* uses wireless data and their performances are limited. Visual noise makes it difficult for some data to get correct pseudo visual labels to participate in training and causes the final model to fail to correctly match some difficult video pairs (Fig. 7).

In Table 2, we compare MGM with existing graph neural networks GCN [45] and GAT [46] by replacing MGM in MMGN with GCN and GAT, respectively. GAT also uses the multi-head strategy. As illustrated in Table 2, the performances of *BL + MMGN* using MGM are significantly higher than *BL + MMGN^{G_{CN}}* and *BL + MMGN^{G_{AT}}*. This shows that MGM makes better use of the wireless similarity provided by MMDA. Meanwhile, compared with GAT that adaptively learns the new adjacency matrix from video feature pairs, MGM learns the adjacency matrix from the histogram of wireless similarity more effectively. Besides, we can see that the performances of all methods on these two datasets are consistent, which shows that the simulation data generated for DukeMTMC-VideoReID dataset simulates the real scenarios well.

Prediction of pseudo labels. In Fig. 8(a), we show the percentage of the number of video sequences assigned pseudo visual labels or pseudo multimodal labels to the total number of video sequences. Most of the video sequences are assigned labels and participate in the training

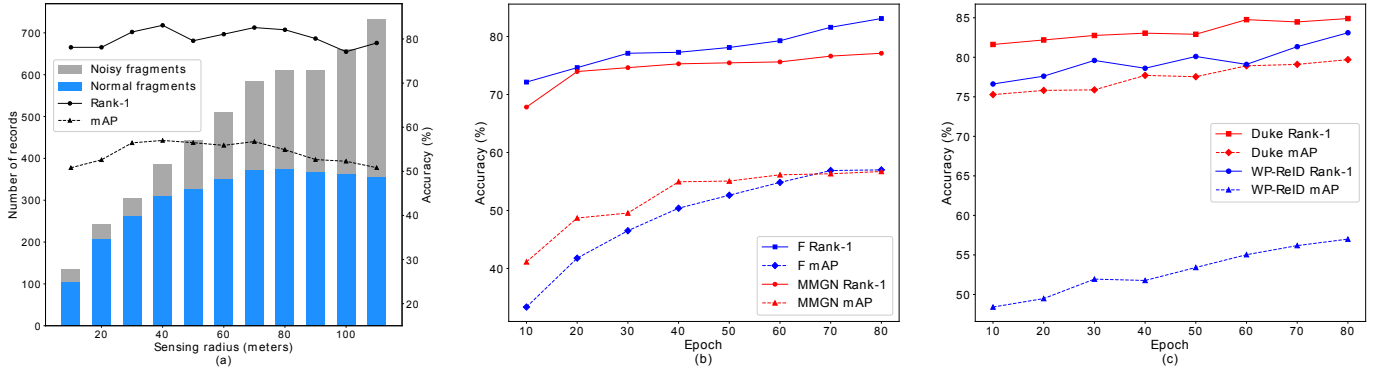


Fig. 9. (a) The influence of the sensing radius of wireless trajectories on the performance of UMTF on WP-ReID dataset. (b) The accuracy changes (%) of model $F(\cdot)$ and MMGN as the number of training epochs increases on WP-ReID dataset. (c) The accuracy changes (%) of model $F(\cdot)$ as the increase of the epochs MMGN participates in the training in UMTF. For example, the value at Epoch = 50 is the accuracy of $F(\cdot)$ that trained for 80 epochs, while the MMGN is removed from UMTF after 50th epoch and wireless data is only involved in the first 50 training epochs.

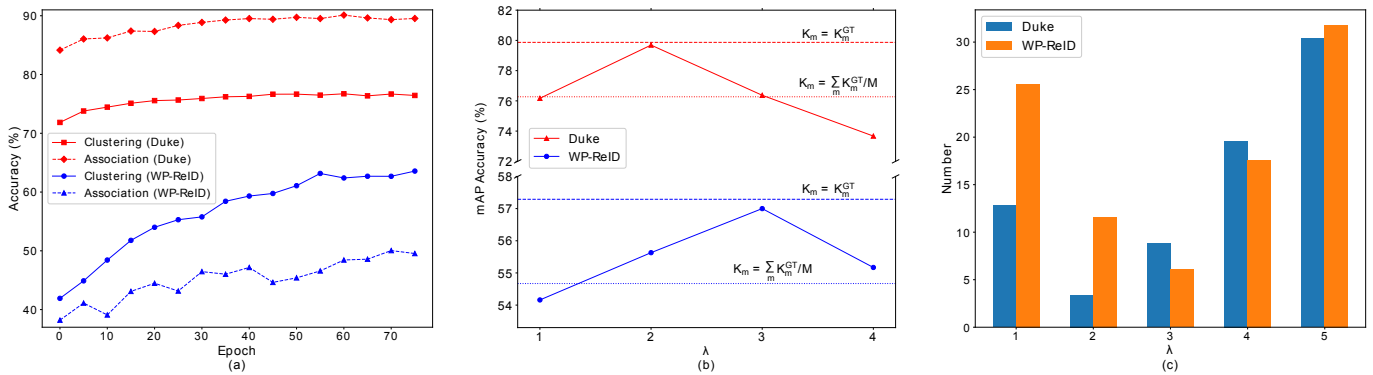


Fig. 10. (a) The accuracy of the clustering results and the accuracy of the multimodal data association between videos and wireless trajectories in MMDA. We use adjusted mutual information (AMI) as the evaluation metric of pseudo-label prediction and clustering. (b) The influence of λ in MMDA on the mAP accuracy of UMTF. $K_m = K_m^{GT}$ means that for m^{th} wireless trajectory, K_m is set to the ground truth person number K_m^{GT} related with it, which is the upper bound of MMDA. $K_m = \sum_m K_m^{GT}/M$ denotes that for all wireless trajectories, the number of clusters is the same and is set to the ground truth average person number related to wireless trajectories. (c) The effect of λ on the difference between the predicted number of clustering centers and the true person numbers. We use Duke to denote the DukeMTMC-VideoReID dataset for brevity.

process of the model. In Fig. 8(b), we show the change of the accuracy of pseudo-label predictions in UMTF with the increase of the number of training epochs. The baseline method only considers visual data and generates pseudo visual labels, whose prediction accuracies are also given in this figure. Adjusted mutual information (AMI) is adopted as the evaluation metric. It can be seen that the prediction accuracies of the two types of pseudo-labels in UMTF are higher than the pseudo-label prediction accuracy of the baseline method. This shows that our method UMTF effectively improves the accuracy of pseudo-label prediction. Meanwhile, when the number of training epochs increases, the prediction accuracies of the two types of pseudo-labels of UMTF increase first and then stabilize in the overall trend. The accuracies of the final label predictions of our method on both datasets are satisfactory.

Influence of the number of wireless trajectories. In Fig. 8(c), we show the effect of the number of wireless signals on the model performance on WP-ReID dataset. The number of video sequences is fixed. When the number of wireless data is 50% in Fig. 8(c), we only randomly select half of the wireless trajectories to participate in the training

of UMTF. The performances of the model $F(\cdot)$ and MMGN are all improved when the number of wireless trajectories increased. This is because the increase in the number of wireless trajectories gives us more clues for multimodal pseudo-label prediction and further reduces the impact of visual noise.

Influence of the sensing radius. We also show the influence of the sensing radius of wireless trajectories on the performance of UMTF in Fig. 9(a). When the sensing radius is small, the number of sensed wireless fragments is small. When the radius is large, the expansion of the sensing area increases the number of sensed wireless fragments. Affected by the size of the sensing area and wireless positioning accuracy, when two cameras are close, there will be some noisy (false-alarm) wireless fragments. For a noisy fragment, the wireless fragment is sensed, but the pedestrian does not appear in the monitoring area of the camera. In WP-ReID, the two closest cameras are only 50 meters apart. It can be seen that the model performs best when the radius is 40 meters. When the sensing radius continues to increase, the performance of the UMTF is stable despite a lot of noisy fragments. The use of visual similarity during clustering

TABLE 3

Performance comparison with the state-of-the-art methods on WP-ReID. Duke means using labeled DukeMTMC-VideoReID as source dataset to pretrain the model. The full-scene labeling means whether to use the GPS coordinate labels of each location in the monitoring scenes of WP-ReID.

Method	WP-ReID						
	Source Dataset	Wireless Data	Full-scene Labeling	mAP	Rank-1	Rank-5	Rank-10
TKP [51]	Duke	×	×	26.1	57.2	73.6	80.1
TKP+RCPM [17]	Duke	✓	✓	47.5	67.2	76.6	83.6
STMP [26]	Duke	×	×	36.8	64.2	80.6	86.1
STMP+RCPM [17]	Duke	✓	✓	60.4	78.1	80.6	83.5
SSG [52]	Duke	×	×	28.2	63.7	77.1	82.1
SSG+RCPM [17]	Duke	✓	✓	47.8	72.1	79.6	85.1
MMT [53]	Duke	×	×	39.1	72.6	82.1	86.1
MMT+RCPM [17]	Duke	✓	✓	61.6	77.1	82.1	86.6
Baseline	×	×	×	43.1	72.1	86.6	92.0
UMTF	×	✓	×	57.0	83.1	93.5	95.0

TABLE 4

Performance comparison with the state-of-the-art unsupervised methods on DukeMTMC-VideoReID. mAP (%), rank-1, 5, 10, 20 accuracy (%) are reported.

Method	DukeMTMC-VideoReID				
	mAP	R1	R5	R10	R20
EGCNC [54]	68.7	76.5	-	-	-
UTAL [34]	72.1	74.5	88.7	-	96.3
UPR-SSL [39]	69.3	76.4	88.7	91.0	-
Baseline	71.4	77.9	90.7	94.4	96.6
UMTF	79.7	84.9	95.9	96.9	98.3

and the soft association strategy in MMDA reduce the interference of noisy fragments and ensure the stability of MMDA.

Mutual promotion of dual models. In Fig. 9(b), we show the accuracy changes of model $F(\cdot)$ and MMGN during the training of UMTF on WP-ReID dataset. It can be seen that the mAP accuracy of MMGN is higher at the beginning but lower than $F(\cdot)$ after 70 epochs. The rank-1 accuracy of MMGN is consistently lower than that of $F(\cdot)$. To verify whether the MMGN drags down the training of $F(\cdot)$, in Fig. 9(c), we evaluate the impact of the number of epochs MMGN participates in training on the performance of the model $F(\cdot)$. The experimental results show that the performance of $F(\cdot)$ is the highest when the MMGN is fully involved in 80 training epochs. This may be because although the performance of MMGN is sometimes lower than $F(\cdot)$, it can assign correct pseudo multimodal labels to some videos that cannot be distinguished correctly by visual data.

Analysis of MMDA. In the multimodal data association strategy (MMDA), we cluster the video sequences and associate them with wireless trajectories. As shown in Fig. 10(a), we show the accuracy of clustering and the accuracy of multimodal data association as the number of training epoch increases. It can be seen that the accuracy of clustering and the accuracy of data association achieve satisfactory results. Especially on the large DukeMTMC-VideoReID dataset, the accuracies of clustering and data association are more stable and higher.

Influence of λ . As shown in Fig. 10(b), we evaluate the impact of λ on UMTF. According to Eq. (2), λ controls the proportional relationship between the number of clusters K_m and the estimated number of pedestrians related with m^{th} trajectory. The results in Fig. 10(b) show that the performances of UMTF are not sensitive to K_m . By roughly adjusting λ , satisfactory results are obtained on both two datasets. When λ is set to 3 and 2, UMTF achieves the highest performances on WP-ReID and DukeMTMC-VideoReID, respectively. In $K_m = K_m^{\text{GT}}$, K_m is set to the ground truth person number K_m^{GT} , which is the upper bound of the performance of our method. The results show that the performance of our adaptive estimation of K_m is very close to the upper bound. Taking the performance of UMTF on WP-ReID dataset as an example, the performance of UMTF is only 0.29% lower than the results achieved with ground truth person labels when $\lambda = 3$. In $K_m = \sum_m K_m^{\text{GT}}/M$, when we set K_m to the same value for all wireless trajectories, the performances drop on two datasets, which shows that it is necessary to adjust the number of clusters adaptively for the related video sequences of different wireless trajectories. Besides, in Fig. 10(c), we give the difference between the predicted number of clustering centers and the true number of pedestrians. The experimental results show that the deviation of the predicted value from the true value is very small when λ is set to a suitable value. This indicates that Eq. (2) is a good way to estimate the appropriate number of clusters for different wireless trajectories, rather than trying without clues.

4.3 Comparison to the State-of-the-art Methods

We compare the performance of our approach UMTF with other state-of-the-art methods on WP-ReID dataset in Table 3. The method RCPM [17] uses the GPS labels of each location of each scene to obtain the coordinate trajectory of the video sequence and calculate the distance to the wireless trajectory. Unlike [17], our setting only needs to know the positions of cameras. The experimental results show that even if our model is not pre-trained with the labeled source dataset and does not use exhaustive scene labeling, our method still obtains the highest rank-1 accuracy and comparable mAP accuracy. This shows that our setting

for multimodal person re-identification is very effective. Meanwhile, UMTF also effectively integrates multimodal information to train a better model.

As shown in Table 4, compared with the existing unsupervised methods that only rely on visual data, our method has obvious performance advantages on DukeMTMC-VideoReID dataset. This means that the introduction of wireless trajectories to assist unsupervised person re-identification is useful and necessary. In other words, wireless data and visual data can complement each other to reduce the influence of various interference factors.

5 CONCLUSION

In this paper, we propose to use wireless trajectories to assist unsupervised person re-identification under weak scene labeling, *i.e.*, we only need to know the locations of the cameras without labeling the latitude and longitude of each location in the monitoring scenes of cameras. We devise a new unsupervised multimodal training framework (UMTF) to train networks with both wireless data and visual data. UMTF mainly contains a multimodal data association strategy (MMDA) and a multimodal graph neural network (MMGN). MMDA calculates the wireless similarity measurement between video sequences by integrating the multimodal data. MMGN uses the specially designed multimodal graph convolutional module (MGM) to pass messages in the video graph. Through the collaboration between the various modules, UMTF obtains a better person representation model for re-identification. Extensive experiments on WP-ReID and DukeMTMC-VideoReID prove the effectiveness of UMTF.

REFERENCES

- [1] W.-S. Zheng, S. Gong, and T. Xiang, "Reidentification by relative distance comparison," *IEEE Transactions on Pattern Analysis and Machine Intelligence (TPAMI)*, vol. 35, no. 3, pp. 653–668, 2012.
- [2] G. Lisanti, I. Masi, A. D. Bagdanov, and A. Del Bimbo, "Person re-identification by iterative re-weighted sparse ranking," *IEEE Transactions on Pattern Analysis and Machine Intelligence (TPAMI)*, vol. 37, no. 8, pp. 1629–1642, 2014.
- [3] E. Ahmed, M. Jones, and T. K. Marks, "An improved deep learning architecture for person re-identification," in *Proceedings of the IEEE Conference on Computer Vision and Pattern Recognition (CVPR)*, 2015, pp. 3908–3916.
- [4] D. Cheng, Y. Gong, S. Zhou, J. Wang, and N. Zheng, "Person re-identification by multi-channel parts-based cnn with improved triplet loss function," in *Proceedings of the IEEE Conference on Computer Vision and Pattern Recognition (CVPR)*, 2016, pp. 1335–1344.
- [5] H. Liu, J. Feng, M. Qi, J. Jiang, and S. Yan, "End-to-end comparative attention networks for person re-identification," *IEEE Transactions on Image Processing (TIP)*, vol. 26, no. 7, pp. 3492–3506, 2017.
- [6] T. Matsukawa, T. Okabe, E. Suzuki, and Y. Sato, "Hierarchical gaussian descriptors with application to person re-identification," *IEEE Transactions on Pattern Analysis and Machine Intelligence (TPAMI)*, vol. 42, no. 9, pp. 2179–2194, 2019.
- [7] L. Wei, Z. Wei, Z. Jin, Z. Yu, J. Huang, D. Cai, X. He, and X.-S. Hua, "Sif: Self-inspired feature learning for person re-identification," *IEEE Transactions on Image Processing (TIP)*, vol. 29, pp. 4942–4951, 2020.
- [8] J. Zhang, L. Niu, and L. Zhang, "Person re-identification with reinforced attribute attention selection," *IEEE Transactions on Image Processing (TIP)*, vol. 30, pp. 603–616, 2020.
- [9] M. Li, X. Zhu, and S. Gong, "Unsupervised person re-identification by deep learning tracklet association," in *Proceedings of the European Conference on Computer Vision (ECCV)*, 2018, pp. 737–753.
- [10] S. Bak, P. Carr, and J.-F. Lalonde, "Domain adaptation through synthesis for unsupervised person re-identification," in *Proceedings of the European Conference on Computer Vision (ECCV)*, 2018, pp. 189–205.
- [11] Z. Zhong, L. Zheng, S. Li, and Y. Yang, "Generalizing a person retrieval model hetero-and homogeneously," in *Proceedings of the European Conference on Computer Vision (ECCV)*, 2018, pp. 172–188.
- [12] W. Deng, L. Zheng, Q. Ye, G. Kang, Y. Yang, and J. Jiao, "Image-image domain adaptation with preserved self-similarity and domain-dissimilarity for person re-identification," in *Proceedings of the IEEE Conference on Computer Vision and Pattern Recognition (CVPR)*, 2018, pp. 994–1003.
- [13] W. Liang, G. Wang, J. Lai, and J. Zhu, "M2m-gan: Many-to-many generative adversarial transfer learning for person re-identification," *arXiv preprint arXiv:1811.03768*, 2018.
- [14] Z. Zhong, L. Zheng, Z. Luo, S. Li, and Y. Yang, "Invariance matters: Exemplar memory for domain adaptive person re-identification," in *Proceedings of the IEEE Conference on Computer Vision and Pattern Recognition (CVPR)*, 2019, pp. 598–607.
- [15] H.-X. Yu, W.-S. Zheng, A. Wu, X. Guo, S. Gong, and J.-H. Lai, "Unsupervised person re-identification by soft multilabel learning," in *Proceedings of the IEEE Conference on Computer Vision and Pattern Recognition (CVPR)*, 2019, pp. 2148–2157.
- [16] L. Fan, T. Li, R. Fang, R. Hristov, Y. Yuan, and D. Katabi, "Learning long term representations for person re-identification using radio signals," in *Proceedings of the IEEE Conference on Computer Vision and Pattern Recognition (CVPR)*, 2020, pp. 10699–10709.
- [17] Y. Liu, W. Zhou, M. Xi, S. Shen, and H. Li, "Vision meets wireless positioning: Effective person re-identification with recurrent context propagation," in *Proceedings of the ACM International Conference on Multimedia (ACM MM)*, 2020, pp. 1103–1111.
- [18] X. Qian, Y. Fu, Y.-G. Jiang, T. Xiang, and X. Xue, "Multi-scale deep learning architectures for person re-identification," in *Proceedings of the IEEE International Conference on Computer Vision (ICCV)*, 2017, pp. 5399–5408.
- [19] Y. Suh, J. Wang, S. Tang, T. Mei, and K. M. Lee, "Part-aligned bilinear representations for person re-identification," in *Proceedings of the European Conference on Computer Vision (ECCV)*, 2018, pp. 402–419.
- [20] X. Liu, H. Zhao, M. Tian, L. Sheng, J. Shao, S. Yi, J. Yan, and X. Wang, "Hydraplus-net: Attentive deep features for pedestrian analysis," in *Proceedings of the IEEE International Conference on Computer Vision (ICCV)*, 2017, pp. 350–359.
- [21] M. Ye, J. Shen, G. Lin, T. Xiang, L. Shao, and S. C. Hoi, "Deep learning for person re-identification: A survey and outlook," *IEEE Transactions on Pattern Analysis and Machine Intelligence (TPAMI)*, 2021.
- [22] R. Hou, B. Ma, H. Chang, X. Gu, S. Shan, and X. Chen, "Feature completion for occluded person re-identification," *IEEE Transactions on Pattern Analysis and Machine Intelligence (TPAMI)*, 2021.
- [23] Y. Liu, W. Zhou, J. Liu, G.-J. Qi, Q. Tian, and H. Li, "An end-to-end foreground-aware network for person re-identification," *IEEE Transactions on Image Processing (TIP)*, vol. 30, pp. 2060–2071, 2021.
- [24] T. Wang, S. Gong, X. Zhu, and S. Wang, "Person re-identification by discriminative selection in video ranking," *IEEE Transactions on Pattern Analysis and Machine Intelligence (TPAMI)*, vol. 38, no. 12, pp. 2501–2514, 2016.
- [25] D. Chung, K. Tahboub, and E. J. Delp, "A two stream siamese convolutional neural network for person re-identification," in *Proceedings of the IEEE International Conference on Computer Vision (ICCV)*, 2017, pp. 1983–1991.
- [26] Y. Liu, Z. Yuan, W. Zhou, and H. Li, "Spatial and temporal mutual promotion for video-based person re-identification," in *Proceedings of the AAAI Conference on Artificial Intelligence (AAAI)*, vol. 33, no. 01, 2019, pp. 8786–8793.
- [27] Y. Liu, J. Yan, and W. Ouyang, "Quality aware network for set to set recognition," in *Proceedings of the IEEE Conference on Computer Vision and Pattern Recognition (CVPR)*, 2017, pp. 5790–5799.
- [28] X. Li, W. Zhou, Y. Zhou, and H. Li, "Relation-guided spatial attention and temporal refinement for video-based person re-identification," in *Proceedings of the AAAI Conference on Artificial Intelligence (AAAI)*, vol. 34, no. 07, 2020, pp. 11434–11441.

- [29] Y. Yan, J. Qin, J. Chen, L. Liu, F. Zhu, Y. Tai, and L. Shao, "Learning multi-granular hypergraphs for video-based person re-identification," in *Proceedings of the IEEE Conference on Computer Vision and Pattern Recognition (CVPR)*, 2020, pp. 2899–2908.
- [30] L. Zhao, X. Li, Y. Zhuang, and J. Wang, "Deeply-learned part-aligned representations for person re-identification," in *Proceedings of the IEEE International Conference on Computer Vision (ICCV)*, 2017, pp. 3219–3228.
- [31] N. McLaughlin, J. M. Del Rincon, and P. Miller, "Recurrent convolutional network for video-based person re-identification," in *Proceedings of the IEEE Conference on Computer Vision and Pattern Recognition (CVPR)*, 2016, pp. 1325–1334.
- [32] L. Zhang, Z. Shi, J. T. Zhou, M.-M. Cheng, Y. Liu, J.-W. Bian, Z. Zeng, and C. Shen, "Ordered or unordered: A revisit for video based person re-identification," *IEEE Transactions on Pattern Analysis and Machine Intelligence (TPAMI)*, vol. 43, no. 4, pp. 1460–1466, 2020.
- [33] M. Gou, Z. Wu, A. Rates-Borras, O. Camps, R. J. Radke *et al.*, "A systematic evaluation and benchmark for person re-identification: Features, metrics, and datasets," *IEEE Transactions on Pattern Analysis and Machine Intelligence (TPAMI)*, vol. 41, no. 3, pp. 523–536, 2018.
- [34] M. Li, X. Zhu, and S. Gong, "Unsupervised tracklet person re-identification," *IEEE Transactions on Pattern Analysis and Machine Intelligence (TPAMI)*, vol. 42, no. 7, pp. 1770–1782, 2019.
- [35] Y. Chen, X. Zhu, and S. Gong, "Deep association learning for unsupervised video person re-identification," in *The British Machine Vision Conference (BMVC)*, 2018.
- [36] M. Ye, A. J. Ma, L. Zheng, J. Li, and P. C. Yuen, "Dynamic label graph matching for unsupervised video re-identification," in *Proceedings of the IEEE International Conference on Computer Vision (ICCV)*, 2017, pp. 5142–5150.
- [37] J. Wu, Y. Yang, H. Liu, S. Liao, Z. Lei, and S. Z. Li, "Unsupervised graph association for person re-identification," in *Proceedings of the IEEE International Conference on Computer Vision (ICCV)*, 2019, pp. 8321–8330.
- [38] Q. Xie, W. Zhou, G.-J. Qi, Q. Tian, and H. Li, "Progressive unsupervised person re-identification by tracklet association with spatio-temporal regularization," *IEEE Transactions on Multimedia (TMM)*, 2020.
- [39] Y. Lin, L. Xie, Y. Wu, C. Yan, and Q. Tian, "Unsupervised person re-identification via softened similarity learning," in *Proceedings of the IEEE Conference on Computer Vision and Pattern Recognition (CVPR)*, 2020, pp. 3390–3399.
- [40] A. Alahi, A. Haque, and L. Fei-Fei, "Rgb-w: When vision meets wireless," in *Proceedings of the IEEE Conference on Computer Vision and Pattern Recognition (CVPR)*, 2015, pp. 3289–3297.
- [41] S. Papaioannou, H. Wen, Z. Xiao, A. Markham, and N. Trigoni, "Accurate positioning via cross-modality training," in *Proceedings of the ACM Conference on Embedded Networked Sensor Systems (SenSys)*, 2015, pp. 239–251.
- [42] B. Korany, C. R. Karanam, H. Cai, and Y. Mostofi, "Xmodal-id: Using wifi for through-wall person identification from candidate video footage," in *Proceedings of the Annual International Conference on Mobile Computing and Networking (MobiCom)*, 2019, pp. 1–15.
- [43] C. X. Lu, X. Kan, B. Du, C. Chen, H. Wen, A. Markham, N. Trigoni, and J. Stankovic, "Autonomous learning for face recognition in the wild via ambient wireless cues," in *Proceedings of the World Wide Web Conference (WWW)*, 2019, pp. 1175–1186.
- [44] C. X. Lu, Y. Li, Y. Xiangli, and Z. Li, "Nowhere to hide: Cross-modal identity leakage between biometrics and devices," in *Proceedings of the World Wide Web Conference (WWW)*, 2020, pp. 212–223.
- [45] T. N. Kipf and M. Welling, "Semi-supervised classification with graph convolutional networks," *arXiv preprint arXiv:1609.02907*, 2016.
- [46] P. Veličković, G. Cucurull, A. Casanova, A. Romero, P. Lio, and Y. Bengio, "Graph attention networks," in *Proceedings of the International Conference on Learning Representations (ICLR)*, 2018.
- [47] A. Vaswani, N. Shazeer, N. Parmar, J. Uszkoreit, L. Jones, A. N. Gomez, L. Kaiser, and I. Polosukhin, "Attention is all you need," in *Advances in Neural Information Processing Systems (NeurIPS)*, 2017.
- [48] A. Hermans, L. Beyler, and B. Leibe, "In defense of the triplet loss for person re-identification," *arXiv preprint arXiv:1703.07737*, 2017.
- [49] Y. Wu, Y. Lin, X. Dong, Y. Yan, W. Ouyang, and Y. Yang, "Exploit the unknown gradually: One-shot video-based person re-identification by stepwise learning," in *Proceedings of the IEEE Conference on Computer Vision and Pattern Recognition (CVPR)*, 2018, pp. 5177–5186.
- [50] K. He, X. Zhang, S. Ren, and J. Sun, "Deep residual learning for image recognition," in *Proceedings of the IEEE Conference on Computer Vision and Pattern Recognition (CVPR)*, 2016, pp. 770–778.
- [51] X. Gu, B. Ma, H. Chang, S. Shan, and X. Chen, "Temporal knowledge propagation for image-to-video person re-identification," in *Proceedings of the IEEE International Conference on Computer Vision (ICCV)*, 2019, pp. 9647–9656.
- [52] Y. Fu, Y. Wei, G. Wang, Y. Zhou, H. Shi, and T. S. Huang, "Self-similarity grouping: A simple unsupervised cross domain adaptation approach for person re-identification," in *Proceedings of the IEEE Conference on Computer Vision and Pattern Recognition (CVPR)*, 2019, pp. 6112–6121.
- [53] Y. Ge, D. Chen, and H. Li, "Mutual mean-teaching: Pseudo label refinery for unsupervised domain adaptation on person re-identification," in *Proceedings of the International Conference on Learning Representations (ICLR)*, 2020.
- [54] X. Wang, R. Panda, M. Liu, Y. Wang, and A. K. Roy-Chowdhury, "Exploiting global camera network constraints for unsupervised video person re-identification," *IEEE Transactions on Circuits and Systems for Video Technology (TCSVT)*, 2020.